Experimental Verification of Guided-Wave Lumped Circuits Using Waveguide Metamaterials

Yue Li* and Zhijun Zhang

Department of Electronic Engineering, Tsinghua University, Beijing 100084, China

(Received 9 September 2017; revised manuscript received 28 January 2018; published 17 April 2018)

Through the construction and characterization in microwave frequencies, we experimentally demonstrate our recently developed theory of waveguide lumped circuits, i.e., waveguide metatronics [Sci. Adv. **2**, e1501790 (2016)], as a method to design subwavelength-scaled analog circuits. In the paradigm of waveguide metatronics, numbers of lumped inductors and capacitors are easily integrated functionally inside the waveguide, which is an irreplaceable transmission line in millimeter-wave and terahertz systems with the advantages of low radiation loss and low crosstalk. An example of multiple-ordered metatronic filters with layered structures is fabricated utilizing the technique of substrate integrated waveguides, which can be easily constructed by the printed-circuit-board process. The materials used in the construction are also typical microwave materials with positive permittivity, low loss, and negligible dispersion, imitating the plasmonic materials with negative permittivity in the optical domain. The results verify the theory of waveguide metatronics, which provides an efficient platform of functional lumped circuit design for guided-wave processing.

DOI: 10.1103/PhysRevApplied.9.044024

I. INTRODUCTION

With the development of the fields of plasmonics and nanophonics, light can be controlled and manipulated in the form of optical lumped circuits, i.e., optical nanocircuits, governed by the circuit theory from electronics [1,2]. Inspired by the concept of metamaterials, the state-of-the-art of electronics is transplanted into the optical domain to design lumped nanocircuits (i.e., optical metatronics) [1,2]. For example, the modularization consideration enables us to build complicated optical nanocircuits by assembling individual subwavelength-scaled lumped elements or building blocks, such as nanocapacitors or nanoinductors, instead of solving the multibody scattering problem. In the paradigm of optical metatronics, a nanoparticle (i.e., with subwavelength-scaled dimensions) with a positive real part of permittivity behaves as a nanocapacitor, and a nanoparticle with a negative real part of permittivity behaves as a nanoinductor [1,2]. Based on these lumped elements, the idea of optical metatronics has been experimentally demonstrated in different optical ranges, for example, midinfrared [3], near-infrared [4], and visible frequencies [5]. Various optical metatronic circuits and devices have been successfully achieved, such as filters [3,4,6–8], antennas [9–11], transmission lines [12–14], transmitted arrays [15], computational devices [16], Wheatstone bridges [17], and laser microcavities [18], just to name a few. The concept of optical metatronics provides a possible pathway for light-matter interaction and light signal processing in the nanoscale.

Analogous to optical metatronics, the methodology of modularization and simplification is transplanted into another platform of waveguide structures, which can be performed in relatively lower frequencies, e.g., the microwave or terahertz range [19], termed as "waveguide metatronics." In the approach of waveguide metatronics, the material dispersion, e.g., Drude dispersion, of plasmonic materials in optical metatronics is imitated by using regular materials (positive permittivity, less dispersion, and low loss) with an engineered structure or boundary [19–21], which are already used to realize epsilon negative or near-zero metamaterials [22–24]. In this way, the optical metatronic circuits are constructed inside the waveguide, following the same design rules, but with a different frequency and materials. In other words, the optical metatronic circuits are reproduced in microwave and millimeter-wave frequencies by waveguide metatronic circuits, as another candidate method to integrate lumped inductors and capacitors inside the waveguide. The merits are a lower radiation loss and lower crosstalk than traditional microstrip transmission lines [19,25,26]. The waveguide metatronic circuits behave as actual lumped circuits by dictating the guided-wave flow, analogous to the conduction current in electronic circuits and displacement current in nanophotonic circuits. The difference of waveguide metatronic circuits compared with existing equivalent lumped circuits of typical discontinuities of the

*To whom all correspondence should be addressed.
lyee@tsinghua.edu.cn

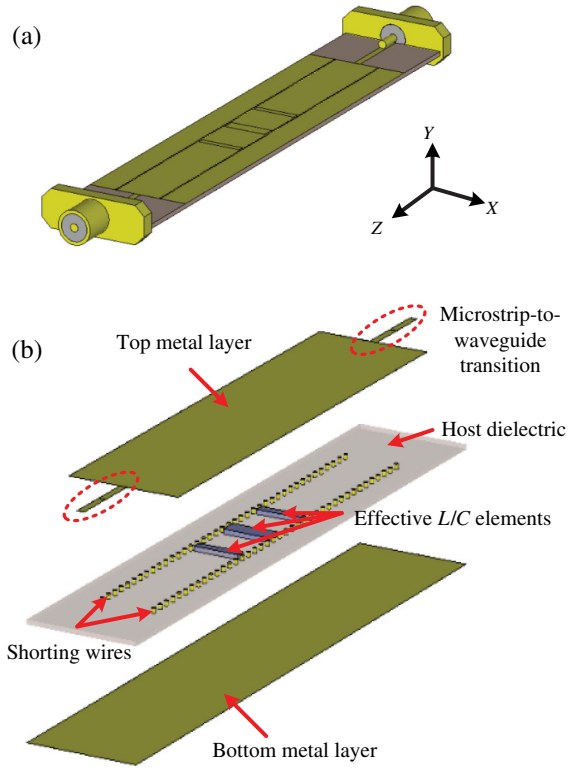

FIG. 1. General configurations of the microwave metatronic circuits using SIW. (a) Experimental setup including an engineered PCB with two SMA connectors. (b) Layered view of the PCB part, consisting of the SIW with several lumped (effective inductive or capacitive) elements and the microstrip-to-waveguide transitions.

waveguide are discussed in Ref. [19]. What is more, we do not mean that the waveguide metatronics will take the place of standard microstrip technology in the microwave region. What we aim to convey is that for the millimeter wave and terahertz systems, e.g., in the recently proposed fifth-generation (5G) communication systems [27,28], the waveguide metatronic circuit is a competitive candidate for lower radiation loss and lower crosstalk advantages [19,25,26].

Here, we carry out the experiments to prove the theoretical work in Ref. [19] as an experimental platform for metatronic circuits and devices. As an example, we experimentally demonstrate the multiordered metatronic filters with layered structures in Ref. [8]. The waveguide metatronic circuits are constructed using the substrate integrated waveguide (SIW) [29,30], which is fabricated based on the typical printed-circuit-board (PCB) process, as illustrated in Fig. 1(a). As shown in the layered view of Fig. 1(b), two rows of shorting wires with a certain period are used to perform the metallic walls or boundary. The lumped elements (i.e., waveguide metatronic inductors or capacitors) are inserted inside host media of the SIW. The waveguide metatronic circuits are connected to the equipment though a pair of microstrip transmission lines (i.e., microstrip-to-waveguide transition) with SMA (subminiature version A) connectors. Because of the intrinsic high-pass property above the cutoff frequency of the waveguide, and the bandwidth limitation of waveguide metatronics (i.e., approximately 5%) [19], the multi-ordered high-pass metatronic filters are the most suitable ones to take the experiment. The inductive elements in the high-pass metatronic filters are realized by using air dielectric. The measured results exhibit that the concept of waveguide metatronics is an effective way to integrate lumped components inside the waveguide for guided-wave processing.

II. WAVEGUIDE METATRONIC ELEMENTS AND CIRCUITS

To begin with, we introduce the lumped elements as the basic building blocks of a waveguide metatronic circuit, analogous to the optical metatronics [1,2]. We consider a rectangular metallic waveguide with a y-polarized TE_{10}-mode incident wave, whose cutoff frequency is determined by the width d. The propagation constant of the TE_{10} mode is [19–21]

$$\beta = k_0\sqrt{\varepsilon_{\text{eff}}}, \tag{1}$$

where k_0 is the wave number in free space, and the effective relative permittivity ε_{eff} of the filled material (with actual relative permittivity ε_{act}) is

$$\varepsilon_{\text{eff}} = \varepsilon_{\text{act}} - \frac{\pi^2 c^2}{d^2\omega^2} = \varepsilon_{\text{act}} - \frac{c^2}{4d^2 f^2}, \tag{2}$$

where c is the speed of light in free space. From Eq. (2), we can see ε_{eff} is a function of the width of the waveguide, performing as the structural dispersion. Here, we use the upper label of L, C, and H to indicate the actual and effective epsilon of the inductor, the capacitor, and the host medium of the waveguide, respectively, such as $\varepsilon^L_{\text{act}}$, $\varepsilon^L_{\text{eff}}$, $\varepsilon^C_{\text{act}}$, $\varepsilon^C_{\text{eff}}$, $\varepsilon^H_{\text{act}}$, and $\varepsilon^H_{\text{eff}}$. By properly selecting the value of d, $\varepsilon^L_{\text{act}}$, and $\varepsilon^C_{\text{act}}$, we can achieve $\varepsilon^L_{\text{eff}} < 0$ and $\varepsilon^C_{\text{eff}} > 0$ simultaneously inside the same waveguide. If the host media of the waveguide is $\varepsilon^H_{\text{act}}$, we need to fulfill the relation of $\varepsilon^L_{\text{act}} < \varepsilon^H_{\text{act}} < \varepsilon^C_{\text{act}}$, making sure that $\varepsilon^L_{\text{eff}} < 0 < \varepsilon^H_{\text{eff}} < \varepsilon^C_{\text{eff}}$. For a thin dielectric slab of $\varepsilon^C_{\text{act}} > 0$ and $\varepsilon^C_{\text{eff}} > 0$ (thickness a is much smaller than the operating wavelength) inside the waveguide, as shown in Fig. 2(a), it behaves as a capacitor, with the capacitance of

$$C = a\varepsilon^C_{\text{eff}}\varepsilon_0 = a\left(\varepsilon^C_{\text{act}} - \frac{c^2}{4d^2 f^2}\right)\varepsilon_0. \tag{3}$$

As shown in Fig. 2(b), the slab with $\varepsilon^L_{\text{act}} > 0$ and $\varepsilon^L_{\text{eff}} < 0$ behaves as an inductor, with the inductance of

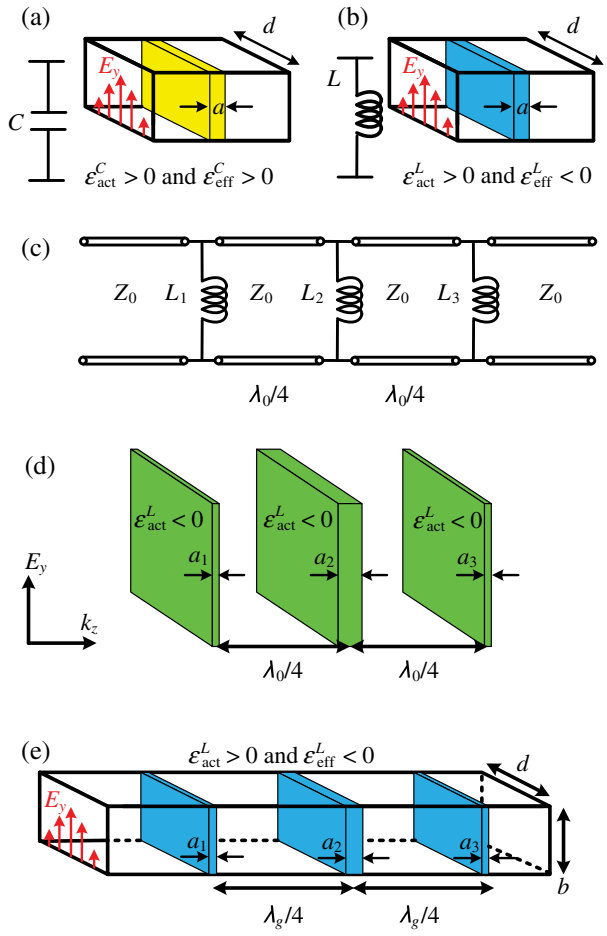

FIG. 2. Waveguide metatronic elements and circuits. (a) Capacitor and (b) inductor of the waveguide metatronics: a thin layer of dielectric inside the waveguide with the TE_{10} mode. The capacitive layer is with a positive actual permittivity and a positive effective permittivity, and the inductive layer is with a positive actual permittivity and a negative effective permittivity. (c) Circuit diagram of the third-ordered high-pass filters with shunt inductors. (d) Optical metatronic circuits realization of (c): layers of inductive dielectric slabs with negative actual permittivity in Ref. [8]. (e) Waveguide metatronic circuit realization of (c) based on the lumped inductive elements in (b).

$$L = -[a(2\pi f)^2 \varepsilon^L_{\text{eff}} \varepsilon_0]^{-1} = -\left[a(2\pi f)^2 \left(\varepsilon^L_{\text{act}} - \frac{c^2}{4d^2 f^2}\right)\varepsilon_0\right]^{-1}. \quad (4)$$

As an example of the metatronic circuit, the circuit diagram and its configuration of a third-ordered high-pass metatronic filter are illustrated in Figs. 2(c) and 2(d) [8]. The circuit diagram in Fig. 2(c) is based on the transmission-line model, with the characteristic impedance of Z_0 (i.e., $\sqrt{\mu_0/\varepsilon_0}$, intrinsic impedance of free space). Three lumped inductors are shunted as three stages in the transmission line with a separation of a quarter wavelength in free space. As shown in Fig. 2(d), the metatronic realization consists of three two-dimensional infinite plasmonic layers [i.e., $\varepsilon(\omega) < 0$], and the thickness of the nth-stage layer is expressed in [8]

$$a_n^{hp} = -g_n[Z_0 2\pi f_{3\text{ dB}} \varepsilon(\omega)\varepsilon_0]^{-1} \quad n = 1, 2, \text{ and } 3, \quad (5)$$

where g_n is the stage coefficient and $f_{3\text{ dB}}$ is the 3-dB cutoff frequency for the high-pass dispersion [26]. The thickness of each layer of the high-pass filter in Fig. 2(d) is subwavelength scaled, and the overall dimension is much smaller than typical optical filters.

In order to imitate the metatronic high-pass filter in Fig. 2(d), the circuit configuration of waveguide metatronics is illustrated in Fig. 2(e). Analogous to the metatronic high-pass filter in free space, the waveguide metatronic high-pass filter is achieved inside a waveguide, whose characteristic impedance and guided wavelength are

$$Z_{\text{wg}} = \sqrt{\mu_0/[\varepsilon^H_{\text{eff}}\varepsilon_0]}, \quad (6)$$

$$\lambda_g = \lambda_0/\sqrt{\varepsilon^H_{\text{eff}}}, \quad (7)$$

where $\varepsilon^H_{\text{eff}}$ is the effective relative permittivity of the host medium of the waveguide, as a function of the operating frequency and the width of the waveguide. Analogous to Eq. (5) for the optical metatronics in free space, the layer thickness of each stage is derived by substituting $\varepsilon(\omega)$ by $\varepsilon^L_{\text{eff}} = \varepsilon^L_{\text{act}} - (c^2/4d^2 f^2_{3\text{ dB}})$, using structural dispersion to imitate material dispersion. We have

$$a_n^{hp} = -g_n\left[Z_{\text{wg}} 2\pi f_{3\text{ dB}}\left(\varepsilon^L_{\text{act}} - \frac{c^2}{4d^2 f^2_{3\text{ dB}}}\right)\varepsilon_0\right]^{-1} \quad n = 1, 2, \text{ and } 3, \quad (8)$$

where $\varepsilon^L_{\text{act}}$ is the actual relative permittivity, a positive real number with no dispersion. Compared to the theoretical thickness of the optical metatronic circuit in Fig. 2(d), the characteristic impedance of the waveguide metatronic circuit in Fig. 2(e) is also dispersive due to the waveguide boundary condition. Therefore, the proposed waveguide metatronic circuits should operate above the cutoff frequency of the waveguide as the lumped circuits for the guided wave.

III. NUMERICAL AND EXPERIMENTAL DEMONSTRATIONS

A series of multiordered metatronic high-pass filters is constructed with layered structures based on the aforementioned design rules. We select typical microwave materials, which are compatible with the standard PCB process. The material for the SIW is Rogers RT6006 as the host medium with $\varepsilon^H_{\text{act}} = 6.15$ and tand $= 0.0027$. The air dielectric is for the inductive layers with $\varepsilon^L_{\text{act}} = 1$.

TABLE I. Tabulated dimensions for the physical implementation of different higher-ordered high-pass filters in waveguide metatronics.

First order	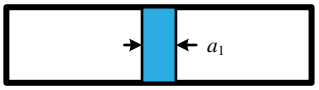	$a_1 = 2.30$ mm
Second order	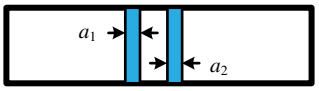	$a_1 = a_2 = 1.63$ mm
Third order	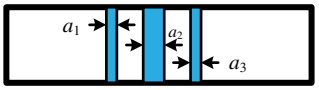	$a_1 = a_3 = 1.15$ mm $a_2 = 2.30$ mm

The detailed configuration of the SIW with the air cavity is illustrated in Fig. S1 of the Supplemental Material [31]. The shorting wires of the SIW are with the diameter of 0.3 mm, and with the period of 0.6 mm. The width (distance between the edges of shorting wires) of the SIW is $d = 6.61$ mm in the X axis, and the height is $b = 0.635$ mm in the Y axis. The cutoff frequency of this SIW is 9.14 GHz, and the effective permittivity is $\epsilon^H_{\text{eff}} = 1$ for $\epsilon^H_{\text{eff}} = 1$ host medium, and $\epsilon^L_{\text{eff}} = -4.15$ for the inductive element. Without loss of generality, the 3-dB cutoff frequency is selected at 10 GHz for the high-pass dispersion. Based on these given parameters, the thickness of each layer for the first, second, and third high-pass filters as waveguide metatronic circuits is theoretically calculated using Eq. (8), and listed in Table I.

In order to prove the design methodology, the waveguide metatronic circuits in Table I are simulated using the commercial software CST MICROWAVE STUDIO. The solver type and meshing method are identically the same as those in Ref. [19]. The input and output ports are both wave ports with the same dimension as the cross section of the SIW. In order to connect the wave port accurately, the first two shorting wires (i.e., the nearest ones to the wave port) are substituted by a metallic block with dimensions of 0.9 mm (Z direction) ×0.3 mm (X direction) ×0.635 mm (Y direction). The detailed circuit structure used in the simulation and configuration of the connect between the wave port and the metallic block are shown in Figs. S2–S5 of the Supplemental Material [31]. The overall length of the PCB is one guided wavelength (30 mm), and the width is 15 mm. Figures 3(c) and 3(c) plot the magnitude distributions of the Y component of the electric field for the third high-pass waveguide metatronic filter at different frequencies in the microwave. The input wave port is at the bottom and the output wave port is on the top. In the stop band, such as 9.5 GHz in Fig. 3(a), most of the energy is reflected to the input and nearly no portion transmits to the output. Therefore, a strong standing wave appears at the input port. As illustrated in Fig. 3(b), at the 3-dB cutoff frequency (i.e., 10 GHz), approximately half of the energy transmits to the output port. And in the passband of 10.5 GHz, all

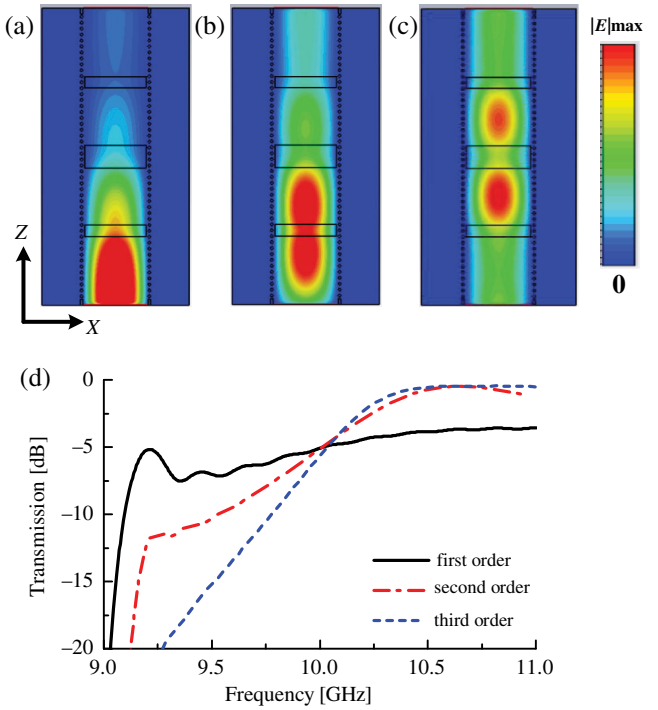

FIG. 3. Numerical simulations of the circuit (i.e., third-ordered high-pass filter) in Fig. 2(e) using the SIW based on the PCB process. Magnitude of the electric field distributions of the Y component on the XZ plane at different frequencies: (a) 9.5 GHz (i.e., in the stop band), (b) 10 GHz (i.e., at 3-dB cutoff frequency), and (c) 10.5 GHz (i.e., in the passband). The distributions are uniform along the Y axis. (d) Transmission coefficients of first-, second-, and third-ordered waveguide metatronic high-pass filters based on the parameters in Table I.

the energy transmits to the output port with almost no reflection, and a strong resonant emerges between the stages. The filed distribution quite agrees well with the counterpart of the optical metatronic circuits, proving the imitation from the optical domain to the microwave domain. The dispersion property of the third-ordered waveguide metatronic high-pass filter is plotted in Fig. 3(d), and compared with the first- and second-ordered cases. First, the high-pass property is clearly seen within the bandwidth of waveguide metatronics. Second, the simulated 3-dB cutoff frequency is approximately 10.1 GHz, at which magnitude of the transmission coefficient is slightly lower than −3 dB due to the loss of the host media. Third, with higher-order filters, the decay rate in the stop band increases, agreeing well with the multiordered optical metatronic filters in Ref. [8]. From the numerical simulations, the waveguide metatronics is able to imitate the circuits property of optical metatronics, operating as a microwave lumped circuit design.

The proof-of-concept demonstration of the waveguide metatronics is provided in the microwave frequency by using the SIW structures based on the PCB fabrication process using copper metal, whose thickness is 20 μm. The host media is Rogers RT6006 with the permittivity of

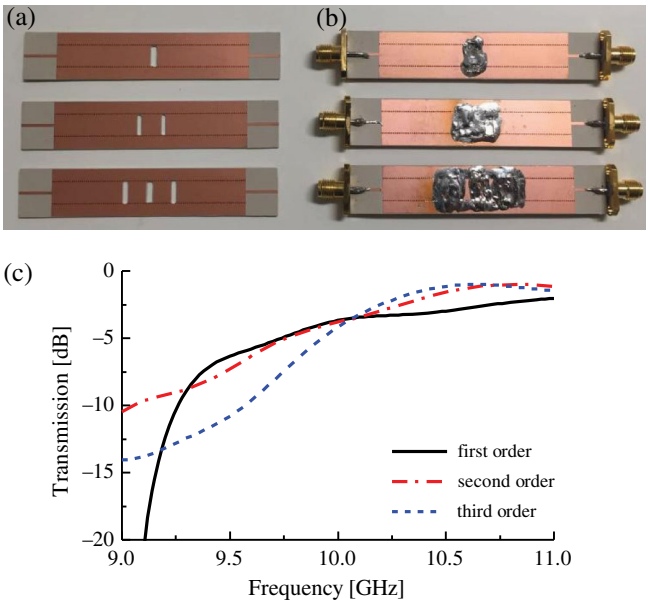

FIG. 4. Experimental demonstration of the theory of waveguide metatronics. (a) Prototype: first, second, and third high-pass filters using the SIW with microstrip-to-waveguide transitions, and the inductive elements use the air dielectric (uncovered) with a negative effective permittivity. The parameters used are listed in Table I. (b) The circuits in (a) for measurement: two SMA are soldered as the input and output ports, and the air dielectric elements are covered with soldered copper tape as a complete waveguide. (c) The measured transmission coefficients of the first-, second-, and third-ordered waveguide metatronic high-pass filters in (b).

$6.15\varepsilon_0$ and the thickness is 0.635 mm. Identical materials and parameters in the numerical simulations, as listed in Table I, are used in the prototype construction and characterization, according to the general structure in Fig. 1(a). The photographs of the measured waveguide metatronic circuits are included in Figs. 4(b) and 4(b). Figure 4(a) shows the SIW structures of first, second, and third high-pass filters with visible air cavities, which perform as the inductive lumped elements, i.e., waveguide metatronic inductors. In Fig. 4(b), copper tapes are soldered on the top and bottom metal layers to cover the air cavities to complete the waveguide structures, as illustrated in Fig. 1(b). If the SIW is inserted with other types of inductive or capacitive elements, different kinds of dielectric can be filled into the air cavities, e.g., powder dialectics. The additional details for the measurement setup are described in Note 1 of the Supplemental Material [31].

The measured magnitude of transmission coefficients of first, second, and third waveguide metatronic high-pass filters are plotted in Fig. 4(c). The detailed retrieval or de-embedded procedure is reported in Notes 2 of the Supplemental Material [31], using a reference SIW without metatronic elements. Comparing the simulated results in Fig. 3(d) and the measured results in Fig. 4(c), a minor difference appears due to the uncertainty of the cable bends and material parameters, with a shift of the 3-dB cutoff frequency in measurement. For the solved transcendental equation in the de-embedded procedure of Notes 2 of the Supplemental Material [31], the solved eigenvalue is valid only above the cutoff frequency of the host waveguide. Besides that, the multiple-ordered property and high-pass dispersion are in good agreement. The measured results prove the design methodology of the waveguide metatronics, as an effective circuit design method in the microwave with the benefits of easily integrating lumped components inside the waveguide.

IV. DISCUSSION AND CONCLUSIONS

In this work, we experimentally demonstrate the concept of waveguide metatronics, which performs as a lumped circuit design method in the microwave and terahertz frequencies. We emphasize the threefold advantages. (i) We experimentally prove that the proposed circuit design method is a reliable, simple, and low-cost manufacture setup, i.e., PCB process, without using the sophisticated fabrication process. (ii) This technique also provides us with an equivalent way to prove design ideas in nanocircuits even though we do not have available "plasmonic" materials. We can emulate specified plasmonic materials using regular materials based on the proposed circuit paradigm. (iii) This technique is based on the lumped circuit theory using waveguide boundary conditions. Therefore, it is another paradigm of microwave or THz circuity with a better performance than the conventional microstrip circuity. For example, in the future (5G) millimeter-wave circuit application, the waveguide is preferred as a transmission line due to the lower loss than the microstrip transmission line [25,26]. Even though the operation bandwidth is limited due to the structural dispersion of the host media, the optical function of a certain metatronic circuit can be imitated or reproduced in the microwave regime by using waveguide metatronics, e.g., the circuits are constructed by the SIW based on the typical PCB process. An example of multiordered metatronic high-pass filters is numerically and experimentally realized in the microwave. The results illustrate that waveguide metatronics has potential applications as a microwave circuit paradigm to imitate the function of certain optical nanocircuits.

ACKNOWLEDGMENTS

This work was supported by the National Natural Science Foundation of China 61771280.

[1] N. Engheta, A. Salandrino, and A. Alù, Circuit Elements at Optical Frequencies: Nanoinductors, Nanocapacitors, and Nanoresistors, Phys. Rev. Lett. **95**, 095504 (2005).

[2] N. Engheta, Circuits with light at nanoscales: Optical nanocircuits inspired by metamaterials, Science **317**, 1698 (2007).
[3] Y. Sun, B. Edwards, A. Alù, and N. Engheta, Experimental realization of optical lumped nanocircuits at infrared wavelengths, Nat. Mater. **11**, 208 (2012).
[4] H. Caglayan, S.-H. Hong, B. Edwards, C. R. Kagan, and N. Engheta, Near-Infrared Metatronic Nanocircuits by Design, Phys. Rev. Lett. **111**, 073904 (2013).
[5] J. Shi, F. Monticone, S. Elias, Y. Wu, D. Ratchford, X. Li, and A. Alù, Modular assembly of optical nanocircuits, Nat. Commun. **5**, 3896 (2014).
[6] Q. Zhang, L. Bai, Z. Bai, P. Hu, and C. Liu, Equivalent-nanocircuit-theory-based design to infrared broad band-stop filters, Opt. Express **23**, 8290 (2015).
[7] H. Liu, Shivanand, and K. J. Webb, Optical circuits from anisotropic films, Phys. Rev. B **79**, 094203 (2009).
[8] Y. Li, I. Liberal, and N. Engheta, Dispersion synthesis with multi-ordered metatronic filters, Opt. Express **25**, 1937 (2017).
[9] A. Alù and N. Engheta, Tuning the scattering response of optical nanoantennas with nanocircuit loads, Nat. Photonics **2**, 307 (2008).
[10] J.-S. Huang, T. Feichtner, P. Biagioni, and B. Hecht, Impedance matching and emission properties of nanoantennas in an optical nanocircuit, Nano Lett. **9**, 1897 (2009).
[11] N. Liu, F. Wen, Y. Zhao, Y. Wang, P. Nordlander, N. J. Halas, and A. Alù, Individual nanoantennas loaded with three-dimensional optical nanocircuits, Nano Lett. **13**, 142 (2013).
[12] T. Baba and T. Ishihara, Analysis of transmission line metamaterials at optical wavelength, Phys. Status Solidi (c) **6**, 327 (2009).
[13] K. Song and P. Mazumder, An equivalent circuit modeling of an equispaced metallic nanoparticles (MNPs) plasmon wire, IEEE Trans. Nanotechnol. **8**, 412 (2009).
[14] G. V. Eleftheriades, EM transmission-line metamaterials, Mater. Today **12**, 30 (2009).
[15] F. Monticone, N. M. Estakhri, and A. Alù, Full Control of Nanoscale Optical Transmission with a Composite Metascreen, Phys. Rev. Lett. **110**, 203903 (2013).
[16] A. Silva, F. Monticone, G. Castaldi, V. Galdi, A. Alu, and N. Engheta, Performing mathematical operations with metamaterials, Science **343**, 160 (2014).
[17] Y. Li, I. Liberal, and N. Engheta, Metatronic analogues of the Wheatstone bridge, J. Opt. Soc. Am. B **33**, A72 (2016).
[18] C. Walther, G. Scalari, M. I. Amanti, M. Beck, and J. Faist, Microcavity laser oscillating in a circuit-based resonator, Science **327**, 1495 (2010).
[19] Y. Li, I. Liberal, C. Della Giovampaola, and N. Engheta, Waveguide metatronics: Lumped circuitry based on structural dispersion, Sci. Adv. **2**, e1501790 (2016).
[20] W. Rotman, Plasma simulation by artificial dielectrics and parallel-plate media, IRE Trans. Antennas Propag. **10**, 82 (1962).
[21] C. Della Giovampaola and N. Engheta, Plasmonics without negative dielectrics, Phys. Rev. B **93**, 195152 (2016).
[22] Y. Li and N. Engheta, Supercoupling of surface waves with ε-near-zero metastructures, Phys. Rev. B **90**, 201107 (2014).
[23] R. Marqués, J. Martel, F. Mesa, and F. Medina, Left-Handed-Media Simulation and Transmission of EM Waves in Subwavelength Split-Ring-Resonator-Loaded Metallic Waveguides, Phys. Rev. Lett. **89**, 183901 (2002).
[24] S. Hrabar, J. Bartolic, and Z. Sipus, Waveguide miniaturization using uniaxial negative permeability metamaterial, IEEE Trans. Antennas Propag. **53**, 110 (2005).
[25] R. E. Collin, *Field Theory of Guided Waves.* (McGraw-Hill, New York, 1960).
[26] David M. Pozar, *Microwave Engineering*, 4th ed. (JohnWiley & Sons, Inc., New York, 2012).
[27] Promotion Group, IMT-2020 (5G)PG White paper, Beijing, 2016.
[28] W. Hong, Z. H. Jiang, C. Yu, J. Zhou, P. Chen, Z. Yu, H. Zhang, B. Yang, X. Pang, M. Jiang, Y. Cheng, M. K. T. Al-Nuaimi, Y. Zhang, J. Chen, and S. He, Multibeam antenna technologies for 5G wireless communications, IEEE Trans. Antennas Propag. **65**, 6231 (2017).
[29] F. Xu, Y. Zhang, W. Hong, K. Wu, and T. Cui, Finite-difference frequency-domain algorithm for modeling guided-wave properties of substrate integrated waveguide, IEEE Trans. Microwave Theory Tech. **51**, 2221 (2003).
[30] L. Yan, W. Hong, G. Hua, J. Chen, K. Wu, and T. Cui, Simulation and experiment on SIW slot array antennas, IEEE Microwave Guided Wave Lett. **14**, 446 (2004).
[31] See Supplemental Material at http://link.aps.org/supplemental/10.1103/PhysRevApplied.9.044024 for the descriptions of the simulation and experimental setup, the measurement method of transition parameters, and the data processing method.